Turbulence and geodesic acoustic mode behavioural studies in ASDEX Upgrade using Doppler Reflectometry

G.D.Conway[1], C.Tröster[1], J.Schirmer[1], W.Suttrop[1], C.Lechte[2], E.Holzhauer[2], B.Scott[1], E.Poli[1], H.Zohm[1] and the ASDEX Upgrade Team

[1]Max-Planck-Institut für Plasmaphysik, EURATOM Association, D-85748 Garching, Germany
[2]Institut für Plasmaforschung, Pfaffenwaldring 31, D-70569 Stuttgart, Germany

e-mail contact of main author: `Garrard.Conway@ipp.mpg.de`

Abstract.   The interaction of turbulence with stationary and oscillating zonal flows is important for understanding the behaviour of turbulent transport in magnetically confined plasmas. Doppler reflectometry has been used on the ASDEX Upgrade tokamak to measure profiles of E_r, its fluctuations and density turbulence properties such as radial correlation lengths L_r and perpendicular $k_\perp$-spectra. In L-mode the turbulence amplitude reduces predominantly at low $k_\perp$ values with radius; while in H-mode, in addition to the low $k_\perp$ drop around the pedestal - coincident with reduced L_r and enhanced E_r shearing - turbulence falls at all $k_\perp$ values with spectral narrowing towards the core region. Turbulence driven geodesic acoustic modes (GAMs) are observed in the ohmic and L-mode plasma edge, but not in H-modes nor deep in the core. The mode frequency scales as sound speed over major radius, but with an additional inverse plasma elongation dependence in the edge. The GAM amplitude increases linear with the temperature gradient (turbulence drive) up to the L to H-mode transition, but displays a complex dependence on the magnetic configuration: shape, elongation, local q value and field-null presence etc.

1. Introduction

A major factor in the performance of magnetically confined plasmas is the role of turbulence driven transport. There are several aspects of the turbulence, not just its amplitude, which impact on the confinement - its spatial and spectral extent (frequency and wavenumber spectra) as well as the non-linear interactions within the turbulence which can generate zonal plasma flows. These turbulence driven zonal and oscillatory flows (geodesic acoustic modes) can feedback onto the turbulence itself (via growth rates and correlation lengths) as well as the underlying equilibrium profiles and gradients, resulting in a complex interdependence. This self-regulating system can be affected by externally driven plasma velocity shears (i.e. momentum injection via neutral beam heating), radial electric fields E_r, plasma collisionality and the magnetic configuration - e.g. elongation, triangularity and the presence of field-null X-points.

In fusion plasma devices, detailed and substantive turbulence measurements still remain a challenge. Microwave Doppler reflectometry, developed on the ASDEX Upgrade tokamak (AUG) for the direct measurement of turbulence rotation velocity $u_\perp$ profiles [1], E_r profiles and its radial shear [2] plus E_r fluctuations [3], has been extended to also permit turbulence wavenumber k-spectra [4], together with simultaneous E_r shear and turbulence radial correlation length L_r measurements [5]. In this paper we report recent results on, specifically, the character and behaviour of turbulence k-spectra in low and high confinement (L and H-mode) regimes across the edge and mid-core region, together with parametric dependence studies of the edge and core geodesic acoustic modes (GAMs) amplitude scaling with the plasma configuration (damping effects) and profile gradients (turbulence drive).

2. Turbulence measurement technique - Doppler reflectometry

Doppler reflectometry is a hybrid diagnostic technique which combines the turbulence wavenumber selectivity of coherent scattering and the radial localization of reflectometry. By deliberately tilting a reflectometer (in the tokamak poloidal plane) to make an angle θ_o to
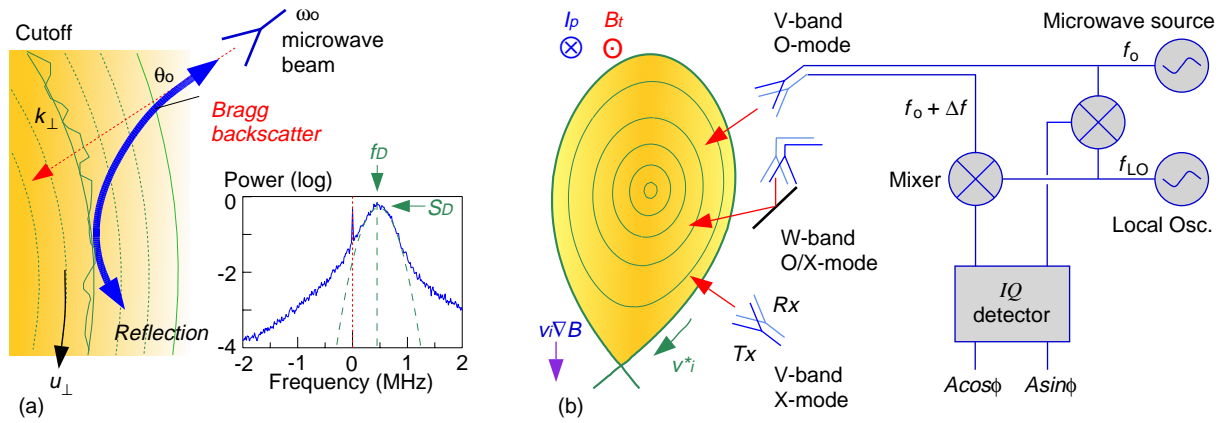
FIG. 1: (a) Doppler reflectometry principle and (b) schematic of system on AUG.

the density gradient the launched microwave beam is refracted and reflected away, as shown in *FIG. 1(a)*, so that only a backscattered signal from the turbulence with a Bragg selected wavenumber $k_\perp = 2k_i = 2Nk_o$ is collected by the receiving antenna. N is the refractive index at the cutoff layer / beam turning point, and $k_o = \omega_o/c$ the probing wavenumber. Further, the backscattered fluctuation spectrum is Doppler frequency shifted $\omega_D = \vec{u} \cdot \vec{k} \approx u_\perp k_\perp$ (for $k_\perp \gg k_\parallel$) by the turbulence moving with the plasma with a perpendicular velocity $u_\perp = v_{E\times B} + v_{\text{turb}}$. Generally $v_{E\times B} \gg v_{\text{turb}}$ at the probed $k_\perp$ which allows extraction of E_r directly from f_D with good accuracy. Alternately, when $v_{E\times B} \sim v_{\text{turb}}$ then information on the turbulence dispersion relation can be obtained [6]. For nearly flat cutoff layers $N^2 \approx \sin^2 \theta_o$, although in practice both the turning point position and N are obtained from ray/beam tracing using experimental density profiles and equilibria. The Doppler shift f_D and spectral intensity $S_D \propto |\tilde{n}(k_\perp)|^2$ (proportional to the density fluctuation at the probed $k_\perp$) are obtained by fitting Gaussians to the complex amplitude spectra [7] - see *FIG. 1(a)* inset.

FIG. 1(b) shows the position of the Doppler reflectometer antennas on ASDEX Upgrade (AUG) together with a system schematic. Currently, three channels are operational: two V-band ($50 - 75$ GHz), one in O-mode and one in X-mode polarization, plus a new W-band ($75 - 105$ GHz) channel in either O or X-mode polarization. All channels probe from the tokamak low-field-side, the V-band using fixed antenna lines-of-sight, while the W-band uses a remote controlled steerable mirror to vary the tilt angle θ_o - and hence the probed $k_\perp \approx 2k_o \sin \theta_o$ [4]. An adjacent antenna collects the backscattered signal which is down-converted using a heterodyne receiver with in-phase and quadrature detection. The complex amplitude signals ($I + iQ = Ae^{i\phi}$) are sampled at 20 MHz for upto 8 seconds [1]. The direct reflection component (normal reflectometry) is minimized by careful design of the antenna radiation pattern so as to optimise the Doppler spectral peak.

3. Turbulence k-spectra

By scanning the antenna tilt angle θ_o using the steerable mirror and the W-band probing frequency (i.e. k_o) a radial profile of the turbulence perpendicular wavenumber spectra between $5 < k_\perp < 25$ cm^{-1} can be measured from roughly the tokamak mid-radius to the separatrix. *FIG. 2* compares typical wavenumber spectra $k_\perp \rho_s$ (where ρ_s is the ion gyro-radius at the sound speed) for L-mode and H-mode conditions (2.5MW NBI heating) at a normalized poloidal flux radius of $\rho_{\text{pol}} \sim 0.78$ - which is well inside of the edge density pedestal top.

All spectra show the expected high-k spectral roll-off. For ohmic and L-mode conditions the spectral decay is typically $k^{-3\pm0.5}$ (in agreement with previous measurements [8]) independent of radius. However, for H-mode the spectral decay steepens, scaling as $k^{-7\pm0.5}$, towards the core region. The overall turbulence also decreases with radius. *FIG. 3* shows radial profiles of the turbulence level in (a) the low $k_\perp \rho_s < 1$ region and (b) the high $k_\perp \rho_s = 2.2$ region for a collection of NBI heated L-mode (open diamond symbols) and H-mode (closed square symbols) discharges. In L-mode the turbulence amplitude in the low $k_\perp$ range falls

FIG. 2: $k_\perp$ spectra for NBI L-mode and H-mode inside the pedestal radius at $\rho_{\mathrm{pol}} \sim 0.78$

towards the core, however, the high $k_\perp$ turbulence range remains constant or even increases slightly. The result is a significant flattening and widening of the low $k_\perp$ part of the spectrum. In H-mode the behaviour is more complicated. Across the tokamak edge region, extending several cm inside of the gradient region (the dashed line indicates the pedestal top radius in *FIG. 3*) the turbulence is predominantly reduced at low $k_\perp$ values. In the steep pedestal gradient region the drop is particularly pronounced. However, further in towards the mid-radius region the high $k_\perp$ level also appears to fall, reaching a factor of 10 reduction or more across the entire wavenumber spectrum, compared to L-mode.
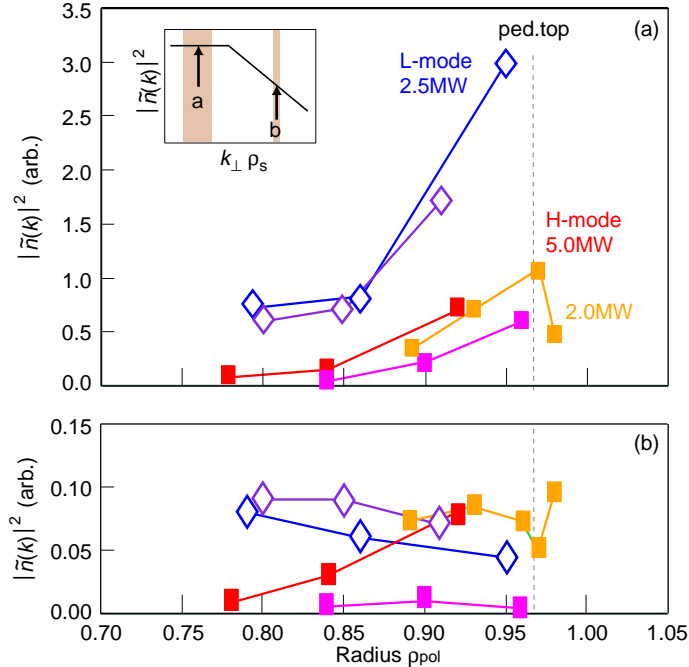

FIG. 3: Radial profiles of $|\tilde{n}(k)|^2$ at (a) low and (b) high $k_\perp$ values for NBI L-mode and H-modes

The spectra in *FIG. 2* show a roll-over in power at the low $k_\perp$ end with a "knee-point" or break in the spectral index around $k_\perp \rho_s \sim 1.5$. A spectral flattening at low k - the condensate range - is expected from theory, and many experiments have reported knee-points between $1 - 6$ rad/cm. *FIG. 4(a)* shows NBI L-mode $k_\perp$ spectra obtained using the steerable tilt antenna and the W-band system ($k_o = 15.7 - 22.0$ rad/cm) for two radial locations $\rho_{\mathrm{pol}} = 0.95$ and 0.86 (red & blue open symbols) with a lower single-null diverted configuration, as shown in *FIG. 4(b)*. The spectra show consistent behaviour at the high $k_\perp$ range, however, the knee-points appear at significantly large $k_\perp$ values. All the low $k_\perp$ points below the roll-over were, rather suspiciously, obtained with very low tilt angles of $\theta_o = -2.3°$ to $+1.8°$. An alternative approach to investigate the low $k_\perp$ region is use a lower probing k_o (V-band: $k_o = 10.5 - 15.7$ rad/cm) and to hold the tilt angle fixed ($\theta_0 \sim 12°$) while varying the plasma triangularity in upper single-null configuration, *FIG. 4(c)*. The correspond-
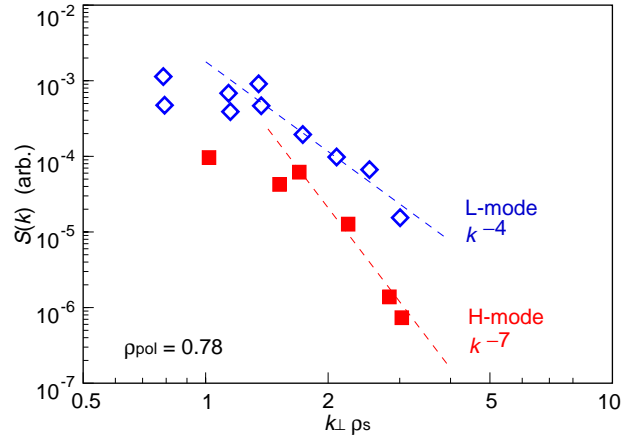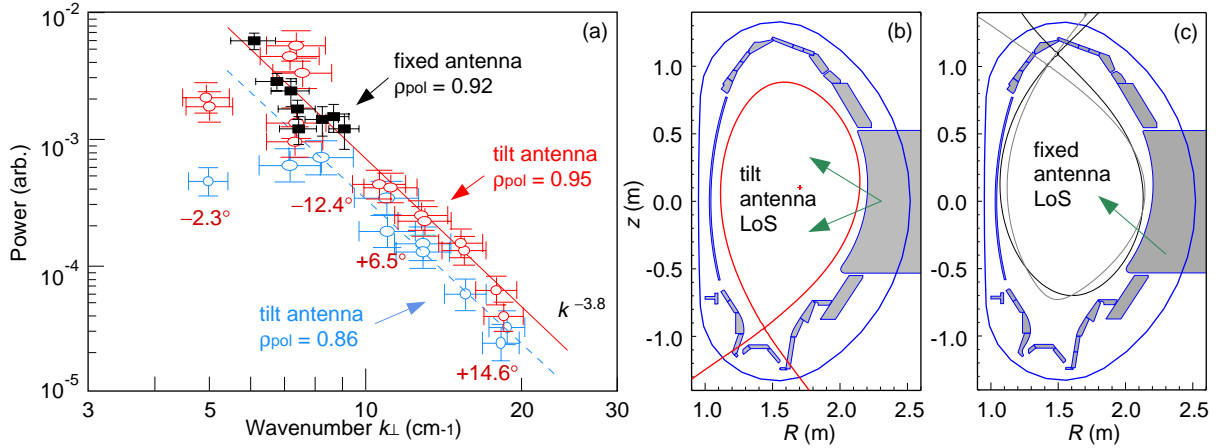
FIG. 4: (a) $k_\perp$-spectra from V-band fixed antenna (black solid symbols) and W-band variable tilt antenna at two radii (red/blue open symbols) for L-mode conditions, and boundary flux surfaces at (b) high triangularity LSN and (c) high and low triangularity USN shots.

ing (rescaled) spectra (black solid symbols in *FIG. 4(a)*) at $\rho_{pol} \sim 0.92$ show the 'inertial range' spectral index extending to lower $k_\perp$. This suggests that the edge turbulence has: (a) a constant nature independent of the plasma triangularity and configuration - at least for these diverted discharges, and (b) that the low tilt angle measurements require additional correction.

The correct interpretation of the Doppler spectra requires knowledge of the diagnostic response function; this has been investigated using 2D full-wave simulation codes. Specifically, modelling results confirm that the spectral power at the Doppler shifted peak scales linearly with the density fluctuation $\tilde{n}/n$ up to roughly 10% levels, independent of the probed $k_\perp$ for reasonable tilt angles of $\theta_o = 5 - 25°$ [9,10]. However, for low tilt angles $\theta_o < 5°$ the spectral peak power at high fluctuation levels ($> 5\%$) can be diminished by factors of $\mathcal{O}(2-4)$ (depending on θ_o and $\tilde{n}/n$) as power is scattered, and hence lost, into higher Bragg angles [9]. These correction factors would bring the low tilt experimental results into line with the fixed tilt values. (Note the interpretation of *FIG. 3(a)* is unaffected). The diagnostic response at the high $k_\perp$ end appears robust. This region is of particular interest for studying electron modes such as electron temperature gradient (ETG) turbulence. Initial attempts to measure an ETG signature have been made using localized ECRH deposition at the plasma mid-radius. There are indications of enhanced fluctuation amplitude at $k_\perp \rho_s \sim 2$ across the edge, although little indication of ∇T_e steepening in the measurement region, possibly due to profile stiffness effects [4].

4. Turbulence radial correlation lengths

The addition of a second reflectometer channel with a slightly different probing frequency, i.e. radial position, but the same tilted antenna line-of-sight allows the simultaneous measurement of the turbulence amplitude, its radial correlation length L_r together with the E_r and its shearing profiles [2]. The cross-correlation of the Doppler backscattered signal has been shown, by extensive 2D full-wave simulation studies, to give a more robust measure of L_r (i.e. relatively insensitive to the fluctuation amplitude and turbulence k-spectrum) than the traditional direct reflected signal obtained with normal incidence reflectometry [5]. Experimentally, in L-mode L_r increases from < 1 cm in the plasma edge to > 3 cm at mid-radius, but, in drops in H-mode by more than a factor of 2 inside of the pedestal top (normalized poloidal flux radius $\rho_{pol} \sim 0.92$), coinciding with an increase in the shear $\partial E_r/\partial r$ in the pedestal from -50 to -300 V cm^{-2} [5].

5. Zonal flows and GAMs - (coherent $v_{E \times B}$ fluctuations)

Since the perpendicular $u_\perp$ velocity contains the $E \times B$ velocity, fluctuations in the radial electric field E_r translate directly to the measured Doppler shift f_D. This makes Doppler reflectometry ideal for the direct measurement of long wavelength coherent $\tilde{E}_r$ modes, such as zonal flows (ZFs) and geodesic acoustic modes (GAMs), with high spatial and temporal resolution. Zonal flows and associated GAMs are non-linear turbulence generated, radially localised ($k_r \neq 0$), $m = n = 0$ mode structured oscillating $E_r \times B$ flows; and their role in moderating the turbulence, via shear de-correlation and energy dissipation, is a topic of high interest.

Previous measurements have identified GAMs in the edge density gradient region of AUG ohmic and L-mode discharges with frequencies between $5-25$ kHz and magnitudes of 1 to 2 orders above the broadband background E_r fluctuations [3]. So far GAMs have not been observed in H-modes. Spatially, two behavioural regions are identified from the mode frequency scaling $\omega = G \, c_s/R_o$ (sound speed $c_s = \sqrt{(T_e + T_i)/M}$ over major radius R_o): (a) the core (inside pedestal radius) of circular limiter configurations where the scale factor $G \approx \sqrt{2}$ - in accordance with simple theory predictions; and (b) the edge ($\rho_{\mathrm{pol}} > 0.95$) where $G \approx 4\pi\{(1 + \kappa_b)^{-1} - \epsilon_o\}$ shows a strong inverse dependence on the plasma boundary elongation κ_b and a constant parameter $\epsilon_o \sim 0.3$ offset which is numerically very close to the average inverse aspect ratio $\epsilon = r/R \sim a/R_o$ over the AUG tokamak edge region. [11]. However, a full test of the ϵ dependence will require further measurements in alternate devices.
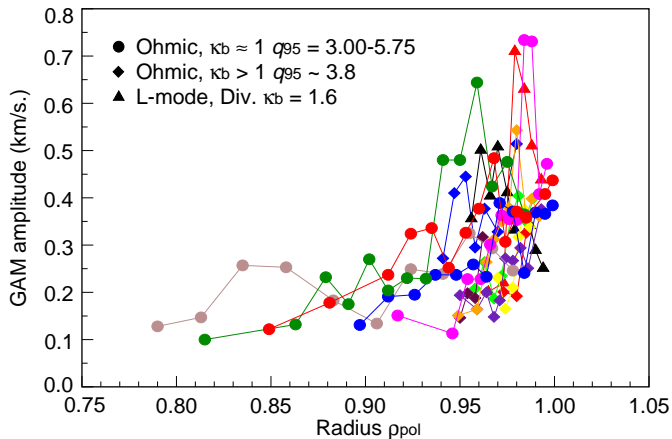

FIG. 5: GAM amplitude vs radial coordinate ρ_{pol} for a range of ohmic and L-mode discharges.

The GAM amplitude also displays strong parameter dependences. *FIG. 5* shows a series of radial profiles of the GAM amplitude (in terms of peak-to-peak velocity displacement) for a range of circular ohmic (circles: $\kappa_b = 1.09$), elongated ohmic (diamonds: $\kappa_b > 1.1$) and diverted L-mode (triangles: $\kappa_b = 1.6$) discharges. Each profile has one or more radial maxima, generally coinciding with the outer edge of plateaus in the GAM frequency profile. There is no clear alignment of the maxima with any rational q surface. The strongest GAM maxima is almost always t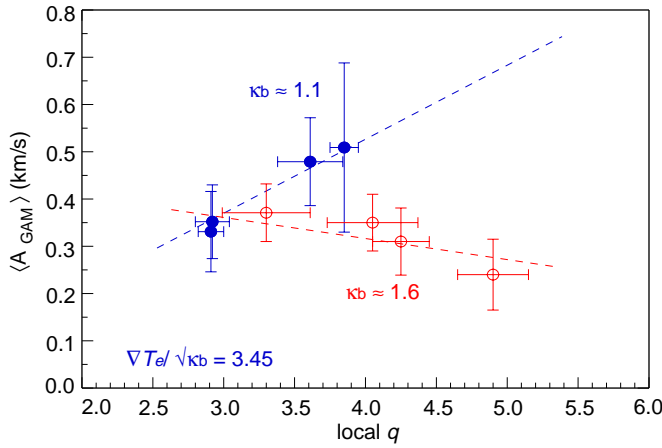owards the edge where safety factor q is larger - consistent with a lower collisionless damping rate $\gamma \propto \exp(-q^2)$. For the diverted (X-point) configurations the density pedestal top (strong second derivative in the profile typically around $\rho_{\mathrm{pol}} > 0.94$) and the separatrix (last-closed flux surface) define the extent of the GAM radial eigenmode structure; while for circular limiter shapes the density pedestal is much reduced with the profile approaching a more parabolic shape, the GAM extends as far in as $\rho_{\mathrm{pol}} \sim 0.75$ - depending on the q profile. The higher the q profile the wider the eigenmode - again consistent with reduced damping with increasing q. In all cases no GAM activity is seen deep in the core region (flat spectra), nor at high collisionality, nor in the open-field SOL region (f^{-1} spectra). The amplitude variation with q is shown in *FIG. 6* for ohmic discharges with a constant normalized temperature gradient of $\nabla T_e/\sqrt{\kappa_b} \approx 3.45$ (indicative of turbulence drive - see below) for circular limiter ($\kappa_b = 1.09$ blue closed symbols) and elongated diverted ($\kappa_b \approx 1.6$ red open symbols) shape.

FIG. 6: Mean GAM amplitude vs local q for circular limiter and elongated divertor discharges.

Here, the GAM amplitude value plotted is the radially averaged peak value taken over the frequency plateau region. For low κ_b circular plasmas this zonal mean GAM amplitude $\langle A_{GAM} \rangle$ increases linearly with the local q value (error bars indicate the amplitude and q variation across the GAM plateau), but becomes less sensitive to q - even decreasing slightly - in diverted high κ_b plasmas. Nevertheless, in both cases the GAM peak position radially moves outward with increasing q.

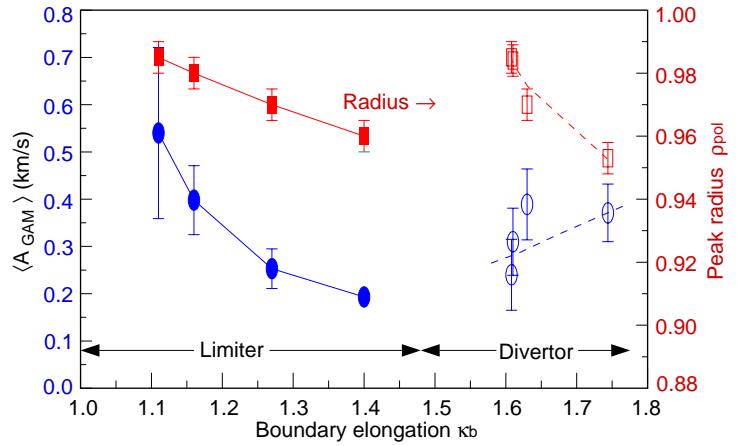The GAM zonal location and amplitude are also affected by the plasma shape. *FIG. 7* shows the zonal mean GAM amplitude $\langle A_{GAM} \rangle$ (blue circles) and the GAM peak radial position (red squares) vs the plasma boundary elongation κ_b for a constant electron temperature gradient $\nabla T_e / \sqrt{\kappa_b} \approx 3.5$. In the AUG tokamak the elongation can be varied from almost circular to mildly elliptic: $1.09 < \kappa_b < 1.48$ in a non-diverted configuration with the plasma touching/limiting on the inner heat-shield. With a single-null diverted shape the elongation can be varied between $1.4 < \kappa_b < 1.75$ with a consequent variation in triangularity. For ohmic limiter discharges (solid symbols) the GAM amplitude drops inversely with κ_b, while for divertor configurations the amplitude rises somewhat with κ_b [12]. In both configurations the GAM peak position also moves radially inward with increasing κ_b, but with an additional outward jump with the formation of the X-point.

An inward movement of the GAM location entails a reduction in the local q value at the GAM peak - and hence larger damping. However, although the direction of GAM amplitude variation with κ_b - decreasing in limiter and increasing in divertor configuration - is consistent with the q behaviour in *FIG. 6*, the consequent magnitude of the amplitude change with q alone is insufficient to account for the $\langle A_{GAM} \rangle$ behaviour with κ_b. This implies additional damping effects; for example, the magnetic shear s, the magnetic shear gradient $\partial s / \partial r$ and $\partial \kappa / \partial r$ all

FIG. 7: Mean GAM amplitude and peak radius vs boundary elongation for limiter and divertor shapes.

increase with increasing elongation which may affect both the underlying turbulence amplitude and the direction (sink or source) of energy transfer from the turbulence to the GAM.

As the GAMs and ZFs are essentially parasitic on the plasma turbulence, the level of turbulence should naturally, in addition to the damping terms, affect the GAM magnitude. For gradient driven turbulence such as drift waves and ITG/TEM type instabilities, the electron temperature radial gradient ∇T_e (converted to a flux surface quantity by normalizing with $\sqrt{\kappa_b}$) should be proportional to the turbulence drive.

The mean GAM amplitude $\langle A_{GAM} \rangle$ vs $\nabla T_e/\sqrt{\kappa}$ is shown in *FIG. 8* for a series of ohmic (blue symbols) and NBI L-mode (red symbols) elongated divertor discharges - with a restricted range of κ_b and q_{95} where the $\langle A_{GAM} \rangle$ sensitivity is weak. The amplitude scaling appears linear with the gradient drive - with an offset, i.e. a critical gradient threshold - through ohmic and L-mode conditions up to the H-mode transition. So far, GAMs have not been observed in well-developed H-modes, possibly due to reduced edge turbulence levels. Nevertheless, what happens across the

FIG. 8: Mean GAM amplitude vs normalized temperature gradient $\nabla T_e/\sqrt{\kappa_b}$ for divertor configuration.

L-H transition remains a crucial question. At the highest L-mode gradient the GAM amplitude is substantial - several tens of percent of the mean flow velocity - and its frequency (a few kHz) is lower than the inverse of the turbulence de-correlation time so it is expected to have a pronounced effect on turbulence eddy shearing. Whether this degree of shearing is sufficient to trigger the suppression of turbulence, and the subsequent absence of GAM activity in the H-mode remains to be demonstrated.
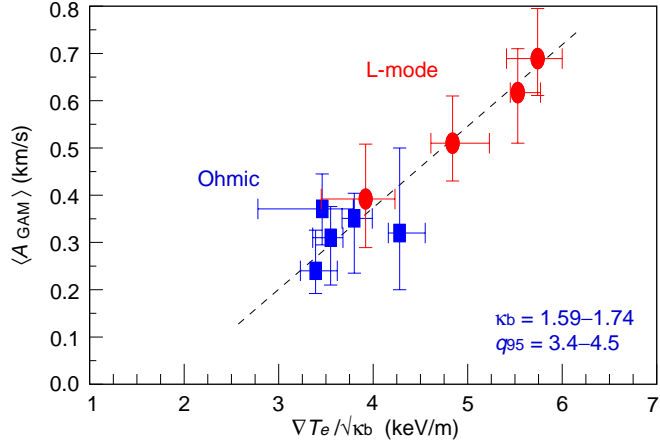
6. Summary and discussion

Microwave Doppler reflectometry is a simple diagnostic technique that can provide radial profiles with good spatial and temporal resolution of a variety of turbulence parameters: the local turbulence amplitude $\tilde{n}_e$, its spectral composition - frequency and wavenumber $k_\perp$, radial correlation lengths L_r, rotation velocities, together with the E_r profile, its shear and its fluctuations. The measurements presented here from the ASDEX Upgrade tokamak show that around the high confinement H-mode density pedestal both the turbulence amplitude and radial correlation length L_r (structure size) are reduced, coincident with enhanced E_r shearing. In the steep density gradient zone and extending some $4 - 5$ cm inside the pedestal top radius, the majority amplitude reduction is at the long wavelength, low $k_\perp$, region. The $k_\perp$-spectral broadening combined with the reduced radial scale lengths L_r indicates the turbulence maintains an approximately isotropic form. Further into the tokamak core the turbulence level reduction is less (although still pronounced) but more uniformly distributed through the $k_\perp$-spectrum. Indeed, in contrast to the L-mode, the $k_\perp$-spectrum becomes narrower towards the core, i.e. the high-k spectral index increases from k^{-3} to k^{-7} or more in H-modes - suggesting a more anisotropic form. With decreasing radius, both the nature of the turbulence - moving from a pressure (EDW) to a temperature gradient (TEM/ITG) dominant drive - and the influence of the edge velocity shear - which, as the measurements show, predominately reduces the longer wavelengths - will change. However, the high-k reduction towards the core indicates additional effects. For example, the density profile flattening inside the pedestal top may actually diminish the shorter wavelength TEM-type turbulence; or turbulence spreading effects, or it may hint at a reduction in non-linear effects such as energy cascades and the geodesic coupling.

The non-linear interactions within the turbulence, e.g. Reynolds stress, drive oscillating and static zonal $E \times B$ flows. In the ohmic and L-mode plasma edge GAM-like coherent $v_{E \times B}$ modes are ubiquitously observed, but, so far not in H-modes. Both the mode frequency and amplitude display complex behaviour. The frequency scales as the expected c_s/R_o, but, in the

edge with an additional inverse plasma elongation dependence. A series of radial plateaus in the GAM frequency together with amplitude maxima, indicate multiple zonal layers a few cm wide. In the core the GAM experiences strong collisionless damping dictated by the q profile: $\gamma \propto \exp(-q^2)$. However, it is more often restricted by a pronounced density pedestal (large $\partial^2/\partial r^2$ in the profiles), as is the case in divertor configurations. The magnetic configuration also determines the parameter dependence; for limiter shapes the GAM amplitude decreases inversely with elongation, but increases linear with q; while for divertor shapes the dependence (although less sensitive) reverses. For divertor configurations the GAM amplitude increases linearly with the normalized electron temperature gradient, i.e. turbulence drive, up to the L to H-mode transition, accompanied by a reduced energy confinement time. The absence of GAMs in well developed H-modes remains an open question: perhaps simply due to lower turbulence levels (drive), or reduced non-linear coupling, or even the high edge rotation shear.

References

[1] CONWAY, G.D. et al., "Plasma rotation profile measurements using Doppler reflectometry", Plasma Phys. Control. Fusion **46** (2004) 951.

[2] SCHIRMER, J. et al., "The radial electric field and its associated shear in the ASDEX Upgrade tokamak", Nucl. Fusion **46** (2006) S780.

[3] CONWAY, G.D. et al., "Direct measurement of zonal flows and geodesic acoustic mode oscillations in ASDEX Upgrade using Doppler reflectometry", Plasma Phys. Control. Fusion **47** (2005) 1165.

[4] TRÖSTER, C.H., "Development of a flexible Doppler reflectometry system and its application to turbulence characterization in the ASDEX Upgrade tokamak", Ph.D. Thesis, Ludwig-Maximilian University. Munich (2008)

[5] SCHIRMER, J. et al., "Radial correlation length measurements on ASDEX Upgrade using correlation Doppler reflectometry", Plasma Phys. Control. Fusion **49** (2007) 1019.

[6] CONWAY, G.D. et al., "Observations on core turbulence transitions in ASDEX Upgrade using Doppler reflectometry", Nucl. Fusion **46** (2006) S799.

[7] CONWAY, G.D. et al., "Doppler reflectometry on ASDEX Upgrade: Foundations and latest results", Proc. 8th Intl. Reflectometer Workshop for Fusion Diagnostics - IRW8 (St.Petersburg, Russia), http://plasma.ioffe.ru/irw8 (2007) pp30-36.

[8] HENNEQUIN, P. et al., "Scaling laws of density fluctuations at high-k on Tore Supra", Plasma Phys. Control. Fusion **46** (2004) B121.

[9] LECHTE, C. et al., "Full-wave Doppler reflectometry simulations in 2D", Proc. 8th Intl. Reflectometer Workshop for Fusion Diagnostics - IRW8 (St.Petersburg, Russia), http://plasma.ioffe.ru/irw8 (2007) pp67-73.

[10] BLANCO, E. and ESTRADA, T., "Study of Doppler reflectometry capability to determine the perpendicular velocity and the k-spectrum of the density fluctuations using a 2D full-wave code", Plasma Phys. Control. Fusion **50** (2008) 095001.

[11] CONWAY, G.D. et al., "Frequency scaling and localization of geodesic acoustic modes in ASDEX Upgrade", Plasma Phys. Control. Fusion **50** (2008) 055009.

[12] CONWAY, G.D. et al., "Amplitude behaviour of geodesic acoustic modes in the ASDEX Upgrade tokamak", Plasma Phys. Control. Fusion **50** (2008) 085005.